Thesis Title

A thesis submitted to the University of Manchester for the degree of
Doctor of Philosophy
in the Faculty of Science and Engineering

2022

Damian Crosby
Department of Mechanical, Aerospace and Civil Engineering

Contents

Word Count: X

List of figures

List of tables

List of publications

Publications go here.

List of abbreviations

2D Two Dimensional

3D Three Dimensional

COM Centre of Mass

DLS Damped Least Squares

Abstract

This is abstract text.

Declaration of originality

I hereby confirm that no portion of the work referred to in the thesis has been submitted in support of an application for another degree or qualification of this or any other university or other institute of learning.

Copyright statement

Acknowledgements

Acknowledgements go here.

Chapter 1

Introduction

1.1 Mobile Robot Stability

Stability is a significant issue for mobile robot design. Loss of stability can mean the robot is unable to move and must be reorientated or retrieved, which maybe difficult or impossible in some extreme environments, such as in outer space or a nuclear fuel pool. In the worst case it can result in severe damage or destruction of the robot, and any objects it is carrying. This has become more of an issue as mobile robots have become increasingly fast and agile, often running, jumping and hopping around less controlled environments.

Figure 1.1: Examples of loss of stability in bipedal and quadrupedal robots.

In many ways the consequences of stability loss in mobile robots are analogous to other situations. A human that falls over has to pick themselves up before continuing on, or if they are infirm they may require assistance. Likewise they could also suffer injury, or if walking along the edge of a long drop, fall to cause severe injury or death. A forklift truck or other piece of heavy plant can topple, injuring the driver and causing the damage or destruction of vehicles and materials.

In general, stability from a biomechanical perspective can be divided into two different types, *static* and *dynamic*. While there are numerous ways to define the difference between the two, such as the maximum lyupanov exponent for dynamic stability, the following definitions will be used:

- **Static stability** only considers the uniform force of gravity and assumes no other forces are acting on the object.
- **Dynamic stability** considers other forces and torques on the object, both internal and external, as well as gravity.

A stationary object that has no external forces or torques being applied needs to be statically stable, a moving object, or an object that is having a force or torque applied to it other than gravity, needs to be dynamically stable.

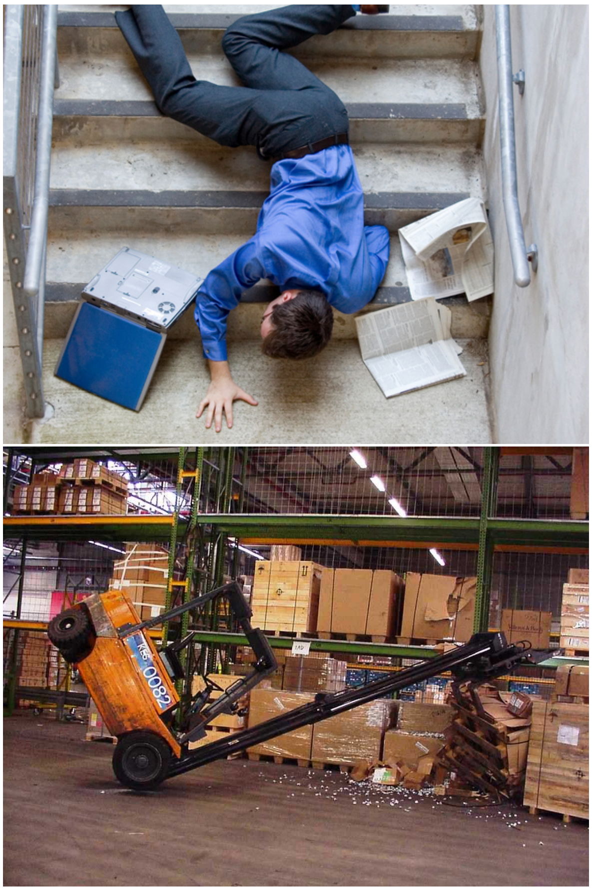

Figure 1.2: Examples of loss of stability (static or dynamic) in a human and forklift truck.

1.1.1 Static Stability

To determine if the robot is statically stable, the gravity axis projection of the center of gravity needs to fall within a defined “support polygon” on the plane perpendicular to the gravity axis plane, as in figure 1.3. If gravity is treated as a constant force along vector g, then the center of mass and center of gravity are equivalent. The center of mass can be calculated for using equation 1.1 for n bodies of masses $m_{1...n}$ and COM positions $\boldsymbol{p_{1...n}}$. If the gravity vector is parallel to any of the basis vectors, then the perpendicular components of the COM/COG can be used to determine the static stability.

$$\mathrm{COG} = \mathrm{COM} = \frac{\sum_{i=1}^{n} m_i \boldsymbol{p_i}}{\sum_{i=1}^{n} m_i} \tag{1.1}$$

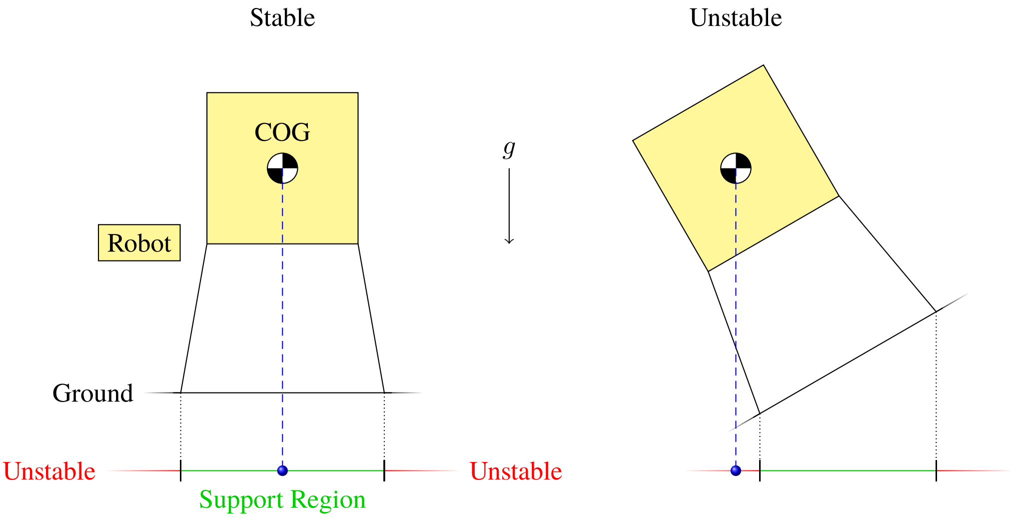

Figure 1.3: 2D representation of the static stability of a legged robot, with the support region defined by the contact points of the legs with the ground. Notice how the orientation of the robot with respect to the gravity axis can move it in and out of the static stability region.

Fundamentally, there are two different methods to maintain static stability:

- Change the region or shape of the support polygon so the gravity axis projection of the center of gravity remains within the bounds of the support polygon.
- Move the gravity axis projection of the center of gravity so it remains within the bounds of the support polygon.

The former method can be considered equivalent to using a walking pole to steady yourself on uneven ground when hiking, the leg of the pole acts as a new vertex that is used to calculate the support polygon, expanding it sufficiently, or placing your foot in front of you when walking. The latter method can be considered equivalent to leaning back to remain upright when falling forward. Leaning back moves the centre of gravity to keep it within the support polygon.

However, just because the center of gravity falls outside of the support polygon does not mean that loss of stability is inevitable, as long as a force or torque applied to the body counteracts the forces and torques induced by the force of gravity in order to maintain stability. This is similar to applying a torque to your ankle when standing on one leg, or a strong wind keeping you upright when leaning forward. If this is the case, then *dynamic* stability is maintained while *static* stability is lost. If the force or torque is removed, then stability is lost. Conversely, forces and torques can also cause loss of stability even if the center of gravity does not fall outside of the support polygon. This is similar to being pushed over, or stopping too quickly and falling forward. So dynamic stability can maintain stability even if static stability is lost, but static stability cannot maintain stability if dynamic stability is lost.

1.1.2 Dynamic Stability

To determine if the robot is dynamically stable,

The concept of the Zero Moment Point, first defined in, is useful for mobile robots to check if dynamic stability will be maintained. It extends the calculation used for static stability by including inertial forces caused by accelerations of the bodies, as shown in figure 1.4. Though it has mostly been utilised for bipedal robots to ensure stability while walking, it is also applicable to quadruped robots, and has even been investigated for the development of a stability warning system in road vehicles [1]. The ZMP is formally defined as the point at which the point where the total of horizontal inertia and gravity forces equals zero. It can be thought of as a *dynamically augmented* version of the gravity axis projection of the center of mass.

Equation 1.2 defines the position of the ZMP for a robot or vehicle with n bodies of masses $m_{1 \dots n}$, COM positions $\boldsymbol{p_{1 \dots n}}$ and COM accelerations $\boldsymbol{\ddot{p}_{1 \dots n}}$, in contact with a planar surface of normal vector $\boldsymbol{n}$ (ZMP cannot be calculated for non-planar surfaces). $\boldsymbol{\tau_{i \dots n}}$ defines the torque acting on each COM, which can be calculated from .

$$\begin{aligned} \boldsymbol{\tau_i} &= \boldsymbol{R_i}\left(\boldsymbol{I_i}\ddot{\theta}_i - \left(\boldsymbol{I_i}\dot{\theta}_i\right) \times \dot{\theta}_i\right) \\ \text{ZMP} &= \frac{\boldsymbol{n} \times \sum_{i=1}^{n}\left(\boldsymbol{p_i} \times m_i\boldsymbol{g} - \boldsymbol{p_i} \times m_i\boldsymbol{\ddot{p}_i} - \boldsymbol{\tau_i}\right)}{\boldsymbol{n} \cdot \left(\left(\sum_{i=1}^{n} m_i\boldsymbol{g}\right) - \left(\sum_{i=1}^{n} m_i\boldsymbol{\ddot{p}_i}\right)\right)} \end{aligned} \tag{1.2}$$

1.1.3 Payload

When a payload is added to the robot, it is equivalent to instantaneously adding an extra body to the robot of mass m_p and position p_p thus changing the COM. Initially the payload will also create an extra contact point with the ground, changing the support polygon so the robot remains statically stable. However, as soon as contact between the payload and ground is severed, the robot can become statically unstable. This does not mean the robot

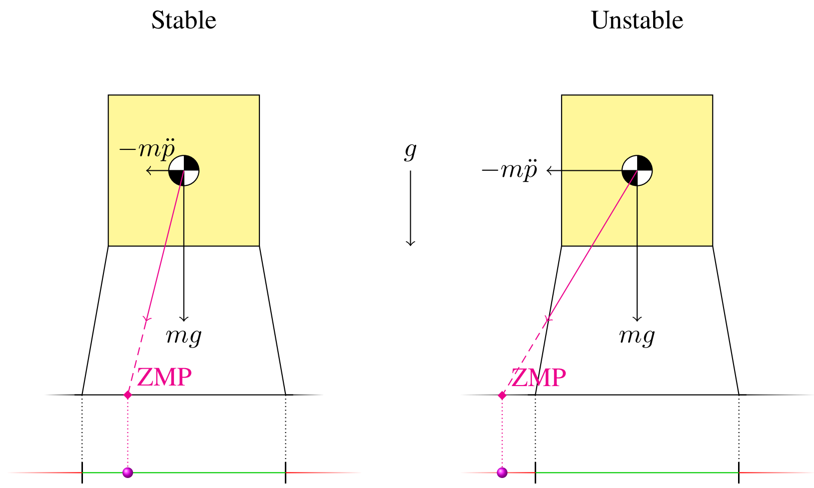

Figure 1.4: 2D representation of the ZMP of a legged robot under horizontal acceleration, with the support region defined by the contact points of the legs with the ground. Notice how increasing the horizontal acceleration of the robot can make it dynamically unstable.

will immediately lose stability, the dynamic forces created picking up the payload may keep the robot dynamically stable, but once the robot is stationary without other forces acting upon it, it may lose stability. The best way to compensate for this is to change the position of the other bodies so the COM remains within the support polygon. This is akin to leaning back when carrying something heavy. But leaning generally has limited range, so can only compensate for lighter payloads. An alternative is needed for heavy payloads.

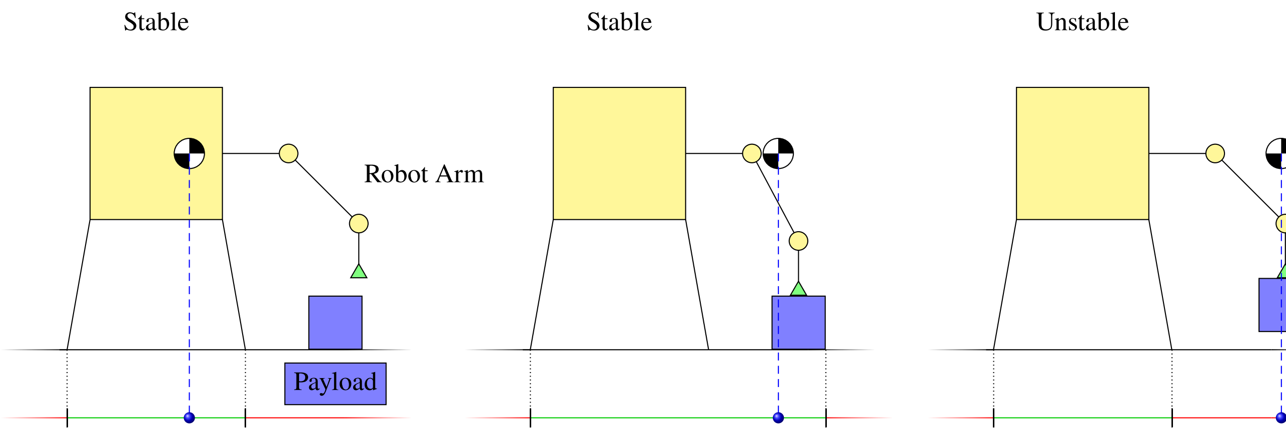

Figure 1.5: 2D representation of the static stability of a legged robot picking up a payload, with the support region defined by the contact points of the arm and legs with the ground. Notice how the payload acts as a contact point until it is lifted off the ground, preventing loss of stability even as the COM/COG is translated due to the mass of the payload.

1.2 Tails

1.2.1 Tails for Stability in the Animal Kingdom

Tails are a common sight in vertebrate animals, a natural extension of the spinal column. While some tails are used purely for grasping, locomotion, communication or decoration, many have some function in maintaining stability.

[2] demonstrates how the domestic cat uses its tail for balance when walking along a narrow beam, which was shifted laterally at a certain velocity by 2.5 cm or 5 cm while they are traversing it. Four cats were trained to walk across the beam, before and after a surgical procedure that severed their spinal cord just above their tail, severely affecting its function. As can be seen from figure 1.6, this procedure caused the cats to fall from the beam far more often than before surgery.

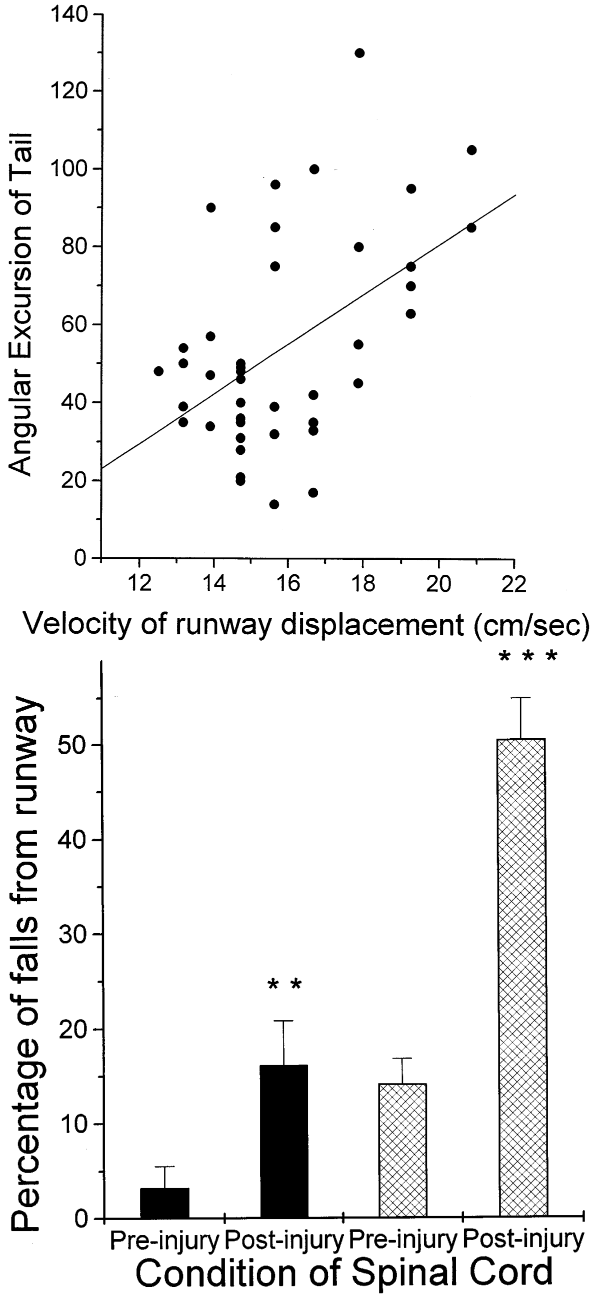

Figure 1.6: Charts from [2] showing how the cat's tail is used to maintain balance on the beam when it is shifted, and how impairing it causes a major loss of stability. Dark bars are a 2.5 cm displacement, cross-hatched bars are a 5 cm displacement.

Case Study 2: Inertial Force/Torque Compensation

Other animals use a tail to compensate for inertial forces and torques induced during a change in velocity, either in magnitude or direction. [3], [4] examines how the cheetah uses its tail to counteract centrifugal force when turning at high speed, and acceleration and braking forces when speeding up and slowing down. They then applied this to a robotic vehicle, which is discussed in section 1.2.2.

Figure 1.7: Images from [3], [4] of a cheetah using its tail during a turn and braking while chasing a lure.

Case Study 3: Aerial Reorientation

Finally, some animals use their tail to remain upright while airborne. [5] examines the aerial stability of the arboreal lizard with an intact tail and with their tail removed. Lizards with the tail removed are unable to maintain their body orientation and do not land cleanly, as can bee seen in figure 1.8. [6] then applies this to a robotic vehicle, discussed in section 1.2.2.

1.2.2 State of the Art Mobile Robots

As many mobile robots have looked at animals for inspiration when it comes to solving various problems with dynamics and locomotion, tails have been used in the development of a significant selection of mobile robots, typically for similar functions as seen in the animal kingdom.

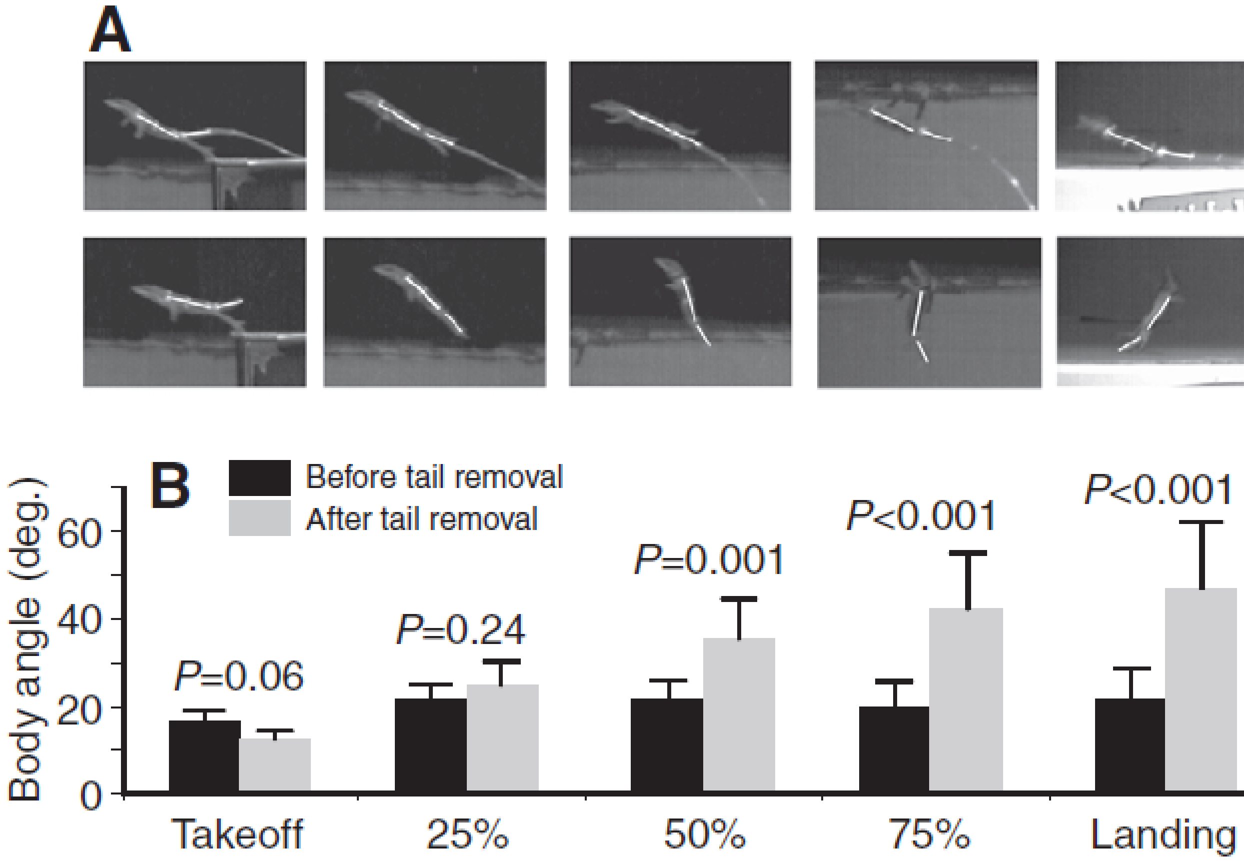

Figure 1.8: Image from [5], showing the body angle of a lizard during a jump, before and after tail removal.

Case Study 1: Balance

[7] uses a tail to keep a legged robot, the “MIT Cheetah”, from falling over when disturbed, in this case the disturbance being a “wrecking ball”, slamming into its side. This can be seen as a similar reaction to the experiments by [2], though it again uses the example of the cheetah in the publication.

Case Study 2: Inertial Force/Torque Compensation

In [3], [4] which also details the functions of the cheetah tail, the robot “Dima” is fitted with a single segment 2-DoF tail which can replicate the motion of the cheetah when this wheeled robot makes a turn at high speed, or accelerates or brakes.

Case Study 3: Inducing Turning Torque

In [8]–[10] a roach like robot is fitted with a single-segment yawing tail. By swinging this tail rapidly to one side or the other during locomotion on a low-friction surface, a reaction torque causes the robot body to rotate and the legs to “skid” on the surface.

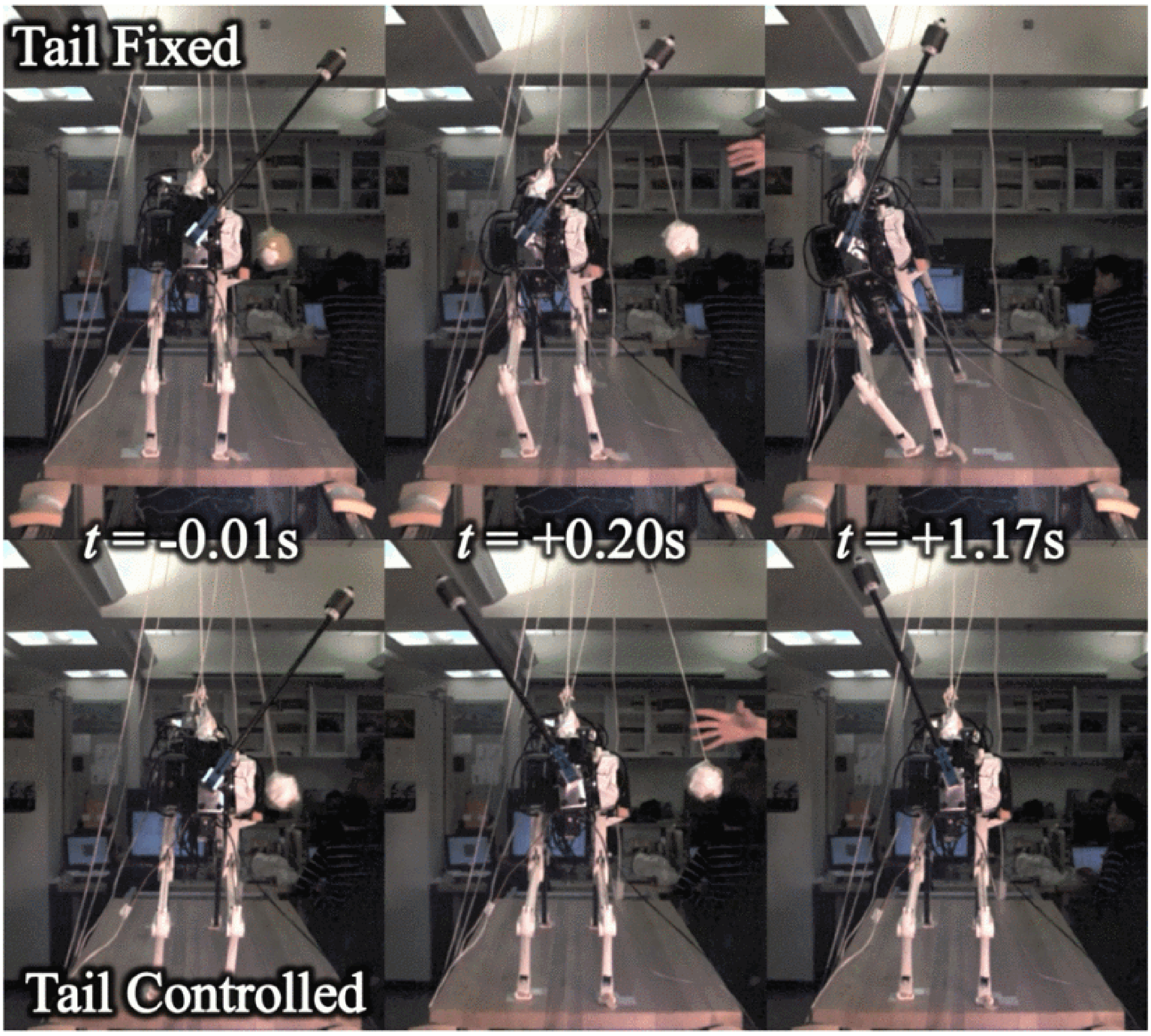

Figure 1.9: Image from [7] showing the difference in body compensation required with and without a moving tail when impacted by a "wrecking ball".

Case Study 4: Aerial Reorientation

In [11] a tail is used to maintain the pitch orientation of a robot when it is dropped from a height, by inducing torques on the body while airborne. They also consider the effect of tail contact against a surface (such as a wall) to increase the torque on the body. Similar studies in publications such as [12] also examine the same technique when a robot has forward momentum (when it drives off a ledge, for example).

References

[1] S. Lapapong, A. Brown, and S. Brennan, "Experimental validation of terrain-aware rollover prediction for ground vehicles using the zero-moment point method," p. 6, Oct. 2020.

[2] C. Walker, C. J. Vierck Jr, and L. A. Ritz, "Balance in the cat: Role of the tail and effects of sacrocaudal transection," *Behavioural brain research*, vol. 91, no. 1-2, pp. 41–47, 1998.

[3] A. Patel and M. Braae, "Rapid turning at high-speed: Inspirations from the cheetah's tail," in *Intelligent Robots and Systems (IROS), 2013 IEEE/RSJ International Conference on*, IEEE, 2013, pp. 5506–5511. DOI: 10.1109/IROS.2013.6697154.

[4] ——, "Rapid acceleration and braking: Inspirations from the cheetah's tail," in *Robotics and Automation (ICRA), 2014 IEEE International Conference on*, IEEE, 2014, pp. 793–799. DOI: 10.1109/ICRA.2014.6906945.

[5] G. B. Gillis, L. A. Bonvini, and D. J. Irschick, "Losing stability: Tail loss and jumping in the arboreal lizard anolis carolinensis," *Journal of Experimental Biology*, vol. 212, no. 5, pp. 604–609, 2009, ISSN: 0022-0949. DOI: 10.1242/jeb.024349. eprint: https://jeb.biologists.org/content/212/5/604.full.pdf. [Online]. Available: https://jeb.biologists.org/content/212/5/604.

[6] T. Libby, T. Moore, E. Chang-Siu, *et al.*, "Tail assisted pitch control in a lizard, robot, and dinosaur," in *Integrative and Comparative Biology*, Oxford univ press inc journals dept, 2001 Evans rd, Cary, NC 27513 USA, vol. 52, 2012, E106–E106. DOI: 10.1038/nature10710.

[7] R. Briggs, J.-W. Lee, M. Haberland, and S.-B. Kim, "Tails in biomimetic design: Analysis, simulation, and experiment," in *Intelligent Robots and Systems (IROS), 2012 IEEE/RSJ International Conference on*, IEEE, 2012, pp. 1473–1480. DOI: 10.1109/IROS.2012.6386240.

[8] A. O. Pullin, N. J. Kohut, D. Zarrouk, and R. S. Fearing, "Dynamic turning of 13 cm robot comparing tail and differential drive," in *Robotics and Automation (ICRA), 2012 IEEE International Conference on*, IEEE, 2012, pp. 5086–5093. DOI: 10.1109/ICRA.2012.6225261.

[9] N. J. Kohut, A. O. Pullin, D. W. Haldane, D. Zarrouk, and R. S. Fearing, "Precise dynamic turning of a 10 cm legged robot on a low friction surface using a tail," in *Robotics and Automation (ICRA), 2013 IEEE International Conference on*, IEEE, 2013, pp. 3299–3306. DOI: 10.1109/ICRA.2013.6631037.

[10] N. Kohut, D. Haldane, D. Zarrouk, and R. Fearing, "Effect of inertial tail on yaw rate of 45 gram legged robot," in *Int. Conf. Climbing Walk. Robot. Support Technol. Mob. Mach*, 2012, pp. 157–164. DOI: 10.1142/9789814415958_0023.

[11] E. Chang-Siu, T. Libby, M. Tomizuka, and R. J. Full, "A lizard-inspired active tail enables rapid maneuvers and dynamic stabilization in a terrestrial robot," in *Intelligent Robots and Systems (IROS), 2011 IEEE/RSJ International Conference on*, IEEE, 2011, pp. 1887–1894. DOI: 10.1109/IROS.2011.6094658.

[12] T. Libby, A. M. Johnson, E. Chang-Siu, R. J. Full, and D. E. Koditschek, "Comparative design, scaling, and control of appendages for inertial reorientation," *IEEE Transactions on Robotics*, vol. 32, no. 6, pp. 1380–1398, 2016. DOI: 10.1109/TRO.2016.2597316.


Dima without tail: 30° turn at 3.5 m/s


Dima with tail: 30° turn at 7.5 m/s

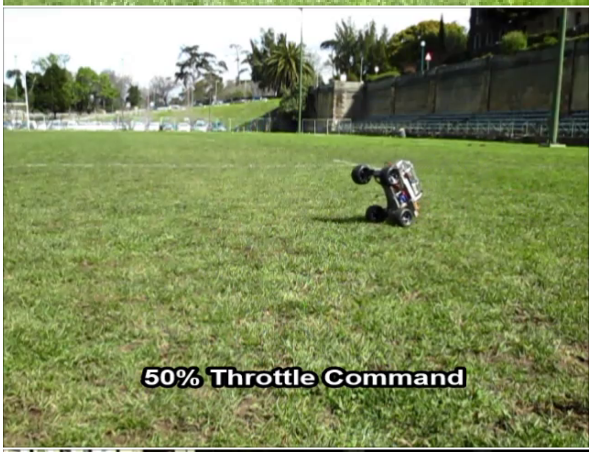
50% Throttle Command


60% Throttle Command

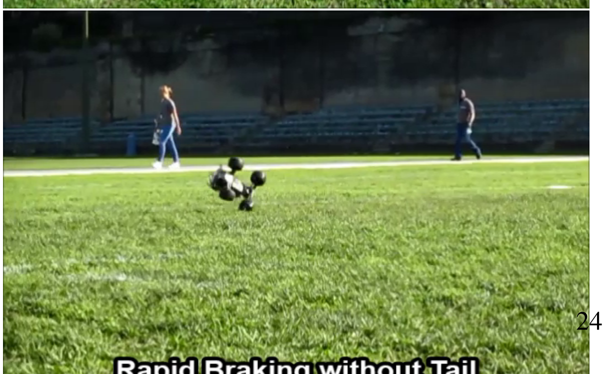
Rapid Braking without Tail

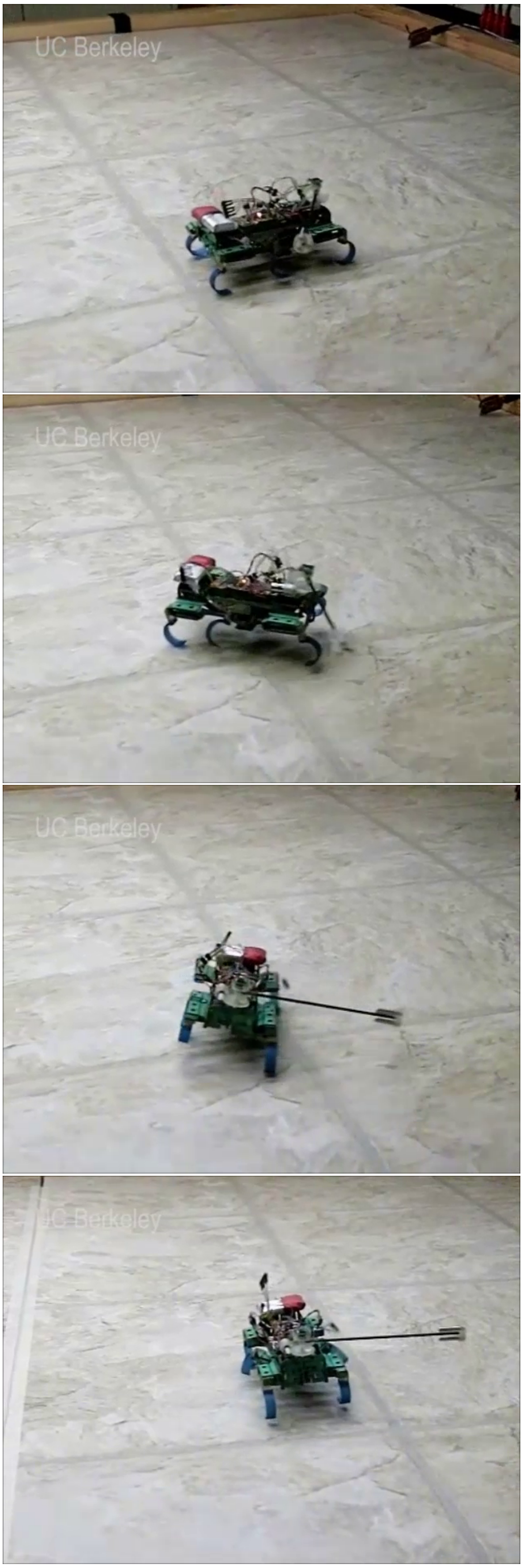

Figure 1.11: Video stills from [9] of the TalyRoACH robot using its tail to change its direction of motion.

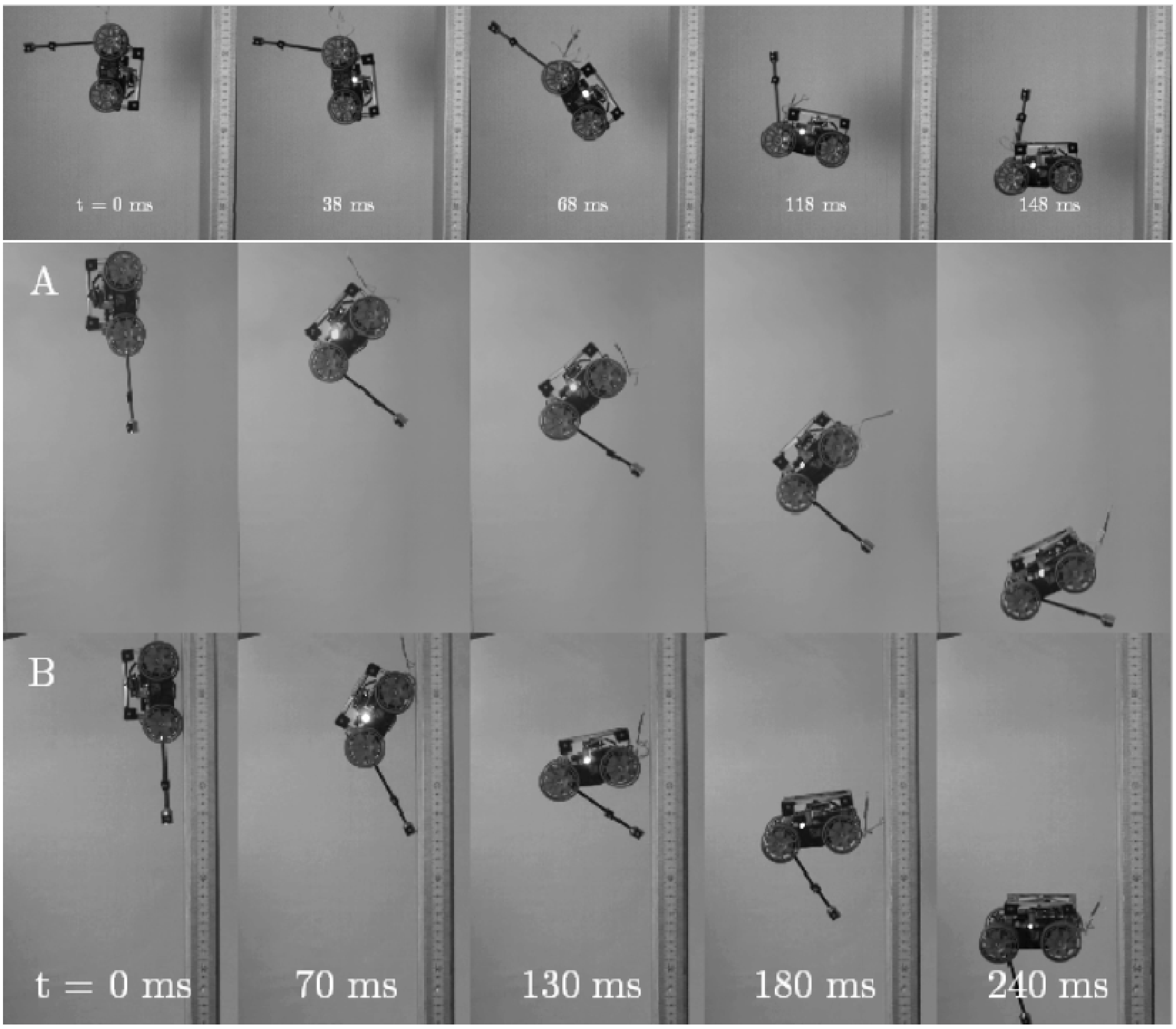

Figure 1.12: Images from [11] of the MSU Tailbot orienting itself after being dropped from a height, and how the tail contacting a wall can improve the orientation range.

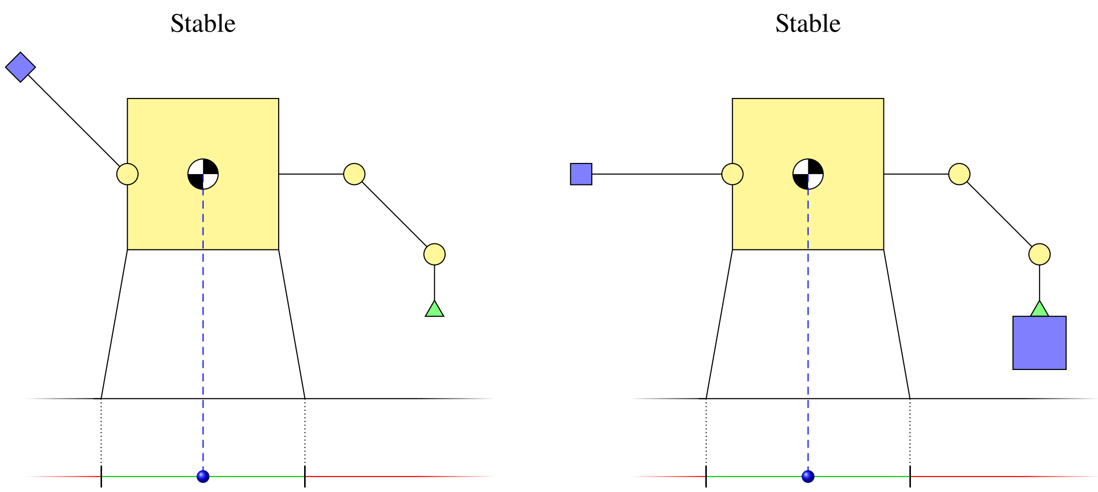

Figure 1.13: 2D representation of the static stability of a legged robot with a weighted tail picking up a payload. By changing the angle of the tail, the postion of its COG can be adjusted in order to compensate for the payload.

Chapter 2

Creating a Configurable Payload for Instability Experiments

2.1 Introduction

In order to generate a diverse set of test data for the experiments in chapter **??**, a configurable payload was conceived, an object that could be configured to have a wide range of masses and COM. A series of test points can then be generated which have a specific mass and COM, and a matching algorithm can be used to find the configuration that mostly closely matches these parameters. The experiments in chapter **??** can then be run with each of these test points to generate the test data.

2.2 Payload Design

The payload consists of a matrix of cubes of various materials packed tightly into a Three Dimensional (3D) printed container. The cubes are designed to be changed after each experimental run to alter the mass and COM of the payload. A lid on the container prevents the cubes from falling out during the experiment, and the exterior design of the box may accommodate additional features to improving the handling of the payload by the robot arm.

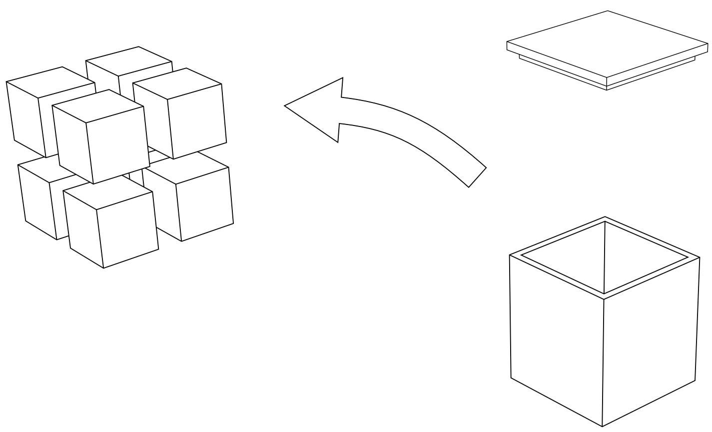

Figure 2.1: Concept drawing of the configurable payload.

Material	Variant	Density (kg m^{-3})
Wood	Pine	860
Plastic	Acrylic	1200
Aluminium	6082	2700
Steel	EN3B	8060

Table 2.1: The materials chosen for the cubes.

2.3 Payload Configuration Space

In order to find a configuration that closely matches a desired test point, first the payload has to be abstracted mathematically, so the mass and COM can be calculated for a given configuration. Firstly we can consider a positive real set of material densities $\mathcal{P} \in \mathbb{R}^+$, each element the density (in kg m^{-3}) of a material to be used:

$$\mathcal{P} = \{\rho_1, \rho_2 \ldots \rho_n \mid \rho_i > 0\} \tag{2.1}$$

Each configuration can then be defined as an $n \times n \times n$ matrix $\boldsymbol{C}$, such that each element is an element of $\mathcal{P}$, where n^3 is the number of cubes in the matrix:

$$\boldsymbol{C} = (c_{ijk}) \in \mathbb{R}^{n^n} \mid (c_{ijk}) \in \mathcal{P} \tag{2.2}$$

2.3.1 Mass and COM functions

To calculate the mass of the configuration, we can take the sum of all the cube densities multiplied by their volume a^3, where a is the cube edge length, plus the container mass m_c:

$$M(\boldsymbol{C}) = \left(\sum_{i=1}^{n}\sum_{j=1}^{n}\sum_{k=1}^{n} c_{ijk}a^3\right) + m_c \tag{2.3}$$

To calculate the COM, we can take the sum of each cube mass multiplied by its position relative to the centroid of the center cube (c_{222}), which can be calculated from the cube indexes ijk, plus the container COM $\boldsymbol{r}_c$ if non-zero:

$$R(\boldsymbol{C}) = \frac{\left(\sum_{i=1}^{n}\sum_{j=1}^{n}\sum_{k=1}^{n} c_{ijk}a^4\left(\begin{bmatrix} i & j & k\end{bmatrix} - n + 1\right)\right) + \boldsymbol{r}_c}{M(\boldsymbol{C})} \tag{2.4}$$

2.4 Test Points

With $\mathcal{Z}$ as the set of all permutations of $\boldsymbol{C}$, test points can be derived from subsets of $\mathcal{Z}$ defined either by logical expressions on $\mathcal{Z}$, or the nearest neighbours of $\mathcal{Z}$ from a set of coordinates. A test point is defined as a $\mathbb{R}^4$ vector containing the target mass and COM concatenated as $\begin{bmatrix} m_i & \boldsymbol{r}_i \end{bmatrix}$.

2.4.1 Extrema Set ($\mathcal{E}$)

The extrema set is designed to test the extremas of the space of $\mathcal{Z}$ for both $M(\mathcal{Z})$ and $R(\mathcal{Z})$. The extrema set if defined from a set of logical constraints. The first two constraints of the set find the maximum and minimum values of the payload mass using $M(\mathcal{Z})$, and the next four constraints use the payload COM using $M(\mathcal{C})$ to get the maximum and minimum values of the x and y component of the COM. Finally, the last four constraints define the diagonal maximum and minimum values where the COM components match $x = y$ or $x = -y$.

$$\mathcal{E} = \left\{ \boldsymbol{x} \subset \mathcal{Z} \mid \begin{cases} M(\boldsymbol{x}) = \max\{M(\mathcal{Z})\} \\ M(\boldsymbol{x}) = \min\{M(\mathcal{Z})\} \\ R(\boldsymbol{x})_x = \max\{R(\mathcal{Z})_x\} \\ R(\boldsymbol{x})_x = \min\{R(\mathcal{Z})_x\} \\ R(\boldsymbol{x})_y = \max\{R(\mathcal{Z})_y\} \\ R(\boldsymbol{x})_y = \min\{R(\mathcal{Z})_y\} \\ R(\boldsymbol{x})_x = \max\{R(\mathcal{Z})_x\} \land R(\boldsymbol{x})_x = R(\boldsymbol{x})_y \\ R(\boldsymbol{x})_x = \min\{R(\mathcal{Z})_x\} \land R(\boldsymbol{x})_x = R(\boldsymbol{x})_y \\ R(\boldsymbol{x})_x = \max\{R(\mathcal{Z})_x\} \land R(\boldsymbol{x})_x = -R(\boldsymbol{x})_y \\ R(\boldsymbol{x})_x = \min\{R(\mathcal{Z})_x\} \land R(\boldsymbol{x})_x = -R(\boldsymbol{x})_y \end{cases} \right\} \tag{2.5}$$

Mass Limited $\mathcal{E}$

When this set was generated, it was found that $M(\mathcal{E}_1)$ was greater than the chosen robot arm could safely lift. Therefore, $M(\boldsymbol{x}) = \max\{M(\mathcal{Z})\}$ in $\mathcal{E}$ was changed to $\begin{bmatrix} m_{max} & 0 & 0 & 0 \end{bmatrix}$ where m_{max} is the safe mass limit that the robot arm can lift. One of the search methods described in section 2.5 can then be used to find the nearest point in configuration space.

2.4.2 Cube Set ($\mathcal{C}$)

The cube set is defined by the vertices of a cube of size b centred around the COM origin $\begin{bmatrix} 0 & 0 & 0 \end{bmatrix}$.

$$\mathcal{C} = \left\{ \boldsymbol{x} \subset \mathcal{C} \mid \begin{bmatrix} \pm\frac{b}{2} & \pm\frac{b}{2} & \pm\frac{b}{2} \end{bmatrix} = \boldsymbol{x} \right\} \tag{2.6}$$

2.4.3 Balanced Set ($\mathcal{B}$)

The balanced set is defined by q points in $\mathcal{C}$ subject to the constraint $R(\boldsymbol{x})_x = 0 \wedge R(\boldsymbol{x})_y = 0$. This can be defined as a "balanced" set as the COM x and y components are both zero. The points are evenly spaced between the maximum and minimum mass as defined in section 2.4.1.

$$\begin{aligned} m_r &= \frac{\max\{M(\mathcal{Z})\} - \min\{M(\mathcal{Z})\}}{q+1} \\ \boldsymbol{z} &= \begin{bmatrix} m_r & 2m_r & \cdots & qm_r \end{bmatrix} \\ \mathcal{B} &= \{\boldsymbol{x} \subset \mathcal{C} \mid z_i = \boldsymbol{x} \wedge R(\boldsymbol{x})_x = 0 \wedge R(\boldsymbol{x})_y = 0\} \end{aligned} \tag{2.7}$$

2.5 Test Point Matching Search Methods

While we are guaranteed an exact result for elements of $\mathcal{E}$ as every element is defined by constraints on known configurations, for $\mathcal{C}$ and $\mathcal{B}$ as the elements are defined numerically, there is no guarantee that any element will have an exact match in solution space. The cardinality of $\mathcal{Z}$ is also important. It is defined as $|\mathcal{Z}| = |\mathcal{P}|^{n^n}$ which increases super exponentially with n. For example, when $|\mathcal{P}| = 4$, $n = 2$ results in 256 permutations and $n = 3$ results in approximately 1.8×10^{16} permutations. It's very clear that when $n > 2$ for non-trivial cardinalities of $\mathcal{P}$, any kind of brute-force method is not computationally tractable. The only exception is for $\mathcal{E}_1$ and $\mathcal{E}_2$, where the solution is trivial as $\mathcal{E}_1 = \boldsymbol{C} \mid \min(\mathcal{P}) \forall c_{ijk}$ and $\mathcal{E}_2 = \boldsymbol{C} \mid \max(\mathcal{P}) \forall c_{ijk}$. Therefore, we investigated both a brute-force nearest neighbour method for when $n = 2$, and a simulated annealing method for when $n = 3$.

2.5.1 Simulated Annealing ($n = 3$)

Simulated annealing [1] is a modification to a gradient descent optimisation that allows the algorithm the chance to "jump out" of local minima early on (even though the approximation becomes temporarily worse). However, as the number of remaining steps decreases, that probability becomes smaller, becoming more and more like gradient descent. First, like any gradient descent algorithm, two things need to be generated, the initial configuration $\boldsymbol{C_0}$, which can be random or manually selected, and the function $\mathcal{N}(\boldsymbol{C})$ which creates a set of all the "neighbours" of $\boldsymbol{C}$. In this case, this can be defined as the subset of $\mathcal{Z}$ where the difference between $\boldsymbol{C}$ and an element of $\mathcal{N}(\boldsymbol{C})$ is one and only one $c_{ijk} \neq c_{ijk}$:

$$\mathcal{N}(\boldsymbol{C}) = \{x \subset \mathcal{Z} \mid \exists!\,(x_{ijk} \neq c_{ijk})\} \tag{2.8}$$

Then the simulated annealing function can be described as follows:

1. Set $\boldsymbol{C}$ to the initial permutation $\boldsymbol{C_0}$.

2. For each of the optimisation steps:

   (a) Set the temperature value t with function $T\left(\frac{k_{max}}{k}\right)$ which takes into account the number of remaining steps.

   (b) Set $\boldsymbol{C}_{new}$ as a random element from the set of all neighbours of $\boldsymbol{C}$ as defined by $\mathcal{N}(\boldsymbol{C})$.

   (c) Use acceptance probability function $P(E(\boldsymbol{C}), E(\boldsymbol{C}_{new}), t)$ where $E(\boldsymbol{C})$ is the energy function (in this case the absolute difference $E(\boldsymbol{C}, g) = |M(\boldsymbol{C}) - g|$ or $E(\boldsymbol{C}, g) = |R(\boldsymbol{C}) - g|$ where g is the target could be used to look for a lower energy state in either mass or COM) to generate a value. Note this function is dependent on the temperature t.

   (d) Compare that value with a random uniformly distributed real number between 0 and 1. If greater than or equal to, then replace $\boldsymbol{C}$ with $\boldsymbol{C}_{new}$. Otherwise, keep it the same.

   (e) Repeat with $\boldsymbol{C}$ until there are no remaining steps.

3. Return the approximated permutation $\boldsymbol{C}$.

$\boldsymbol{C} = \boldsymbol{C}_0$
for $k \leftarrow 1, k_{max}$ **do**
  $t = T\left(\frac{k_{max}}{k}\right)$
  $\boldsymbol{C}_{new} = \mathcal{N}(\boldsymbol{C}) \xleftarrow{R} x$
  if $P(E(\boldsymbol{C}), E(\boldsymbol{C}_{new}), t) \geq x \sim U([0,1])$ **then**
    $\boldsymbol{C} = \boldsymbol{C}_{new}$
  end if
end for
return $\boldsymbol{C}$

Using this algorithm an array of approximate configurations can be easily generated from a desired array of test points. Simulated annealing can also be adapted for multi-objective optimisation [2], so it is possible to generate test points that approximate a desired mass and COM simultaneously.

Cooling Function

2.5.2 Brute-Force Nearest Neighbour ($n = 2$)

If $\mathcal{Z}$ is suitably small, as it is when $n = 2$ then a brute-force method can be used which is guaranteed to find the nearest element to the target within a finite time. This can be done by calculating the L2 norms between the target vector t and all the elements of $\mathcal{Z}$ and finding the minimum. If several elements of $\mathcal{Z}$ have the minimum norm, then one is chosen at random from this set.

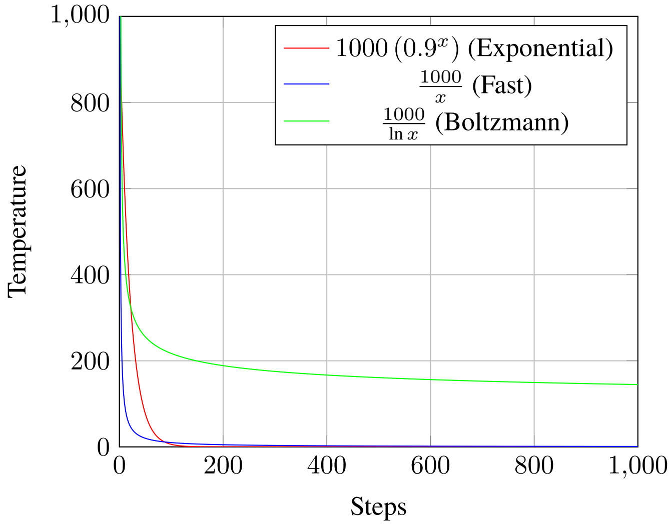

Figure 2.2: Various temperature cooling profiles for simulated annealing, assuming 1000 steps.

$$NN\left(t,\mathcal{Z}\right)=\min\left\{\left\|t-x\right\|_2 \mid \forall x\in\mathcal{Z}\right\} \tag{2.9}$$

2.5.3 Selected Method

Initially an $n = 3$ configuration was used with the acceptance probability function *Rule M* from [2]. This is a weighted blend of two other algorithms defined in the paper, *Rule P* and *Rule W* with a weighting coefficient $\alpha \in (0, 1) \subset \mathbb{R}$. There is also a weighting vector for each element of the test point $\boldsymbol{w} \in \mathbb{R}^4 \mid w_i \in (0, 1)$.

$$P\left(\boldsymbol{x},\boldsymbol{y},\boldsymbol{w},t\right)=\alpha\underbrace{\prod_{i=1}^{m}\min\left\{1,e^{\frac{w_i(x_i-y_i)}{t}}\right\}}_{\text{Rule P}}+(1-\alpha)\underbrace{\min\left\{1,\max_{i=1,\ldots,m}\left\{1,e^{\frac{w_i(x_i-y_i)}{t}}\right\}\right\}}_{\text{Rule W}} \tag{2.10}$$

Unfortunately it was difficult to find a stable and consistent result even after a long time running the algorithm.

Therefore as an alternative, the $n = 2$ configuration was used, with larger cubes to compensate. This successfully produced all three test point sets, after some small adjustments of b in order to get closer to a single configuration for each point of $\mathcal{C}$.

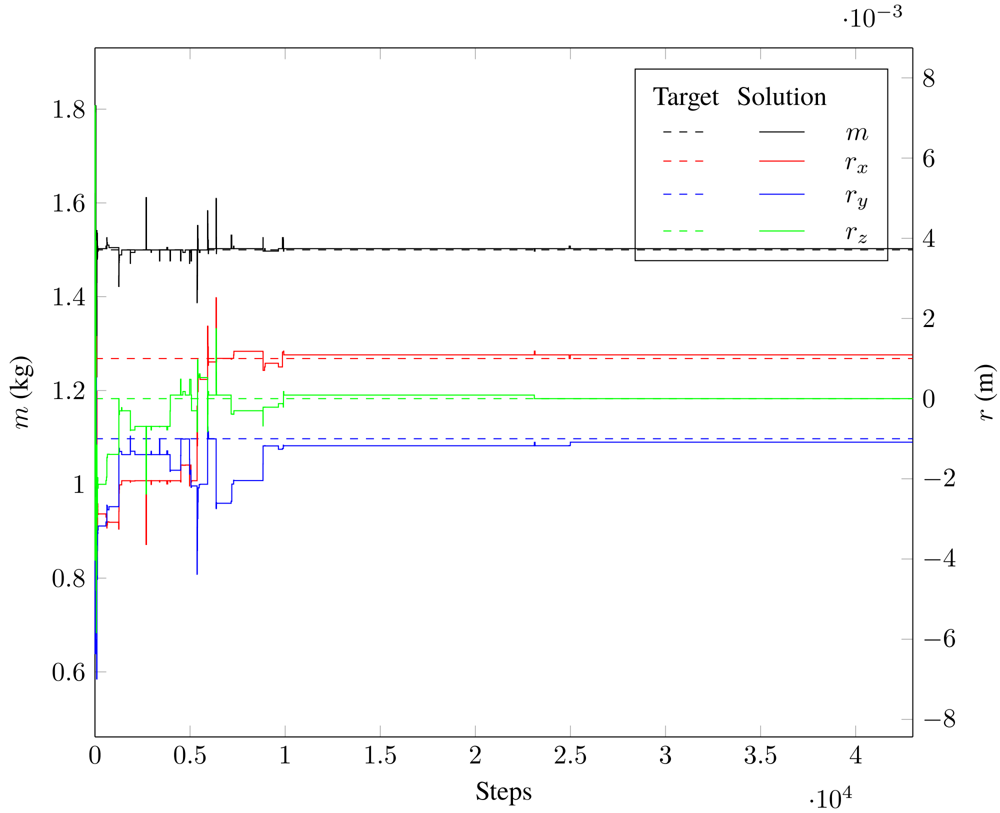

Figure 2.3: Simulated annealing output for the target $[1.5 \quad 0.001 \quad 0.001 \quad 0.001]$ with $\alpha = 0.997$ and even weighting $w_m, \boldsymbol{w_r} = 0.25$ for 4.3×10^4 steps.

m	$\boldsymbol{r}$
Extrema Set ($\mathcal{E}$)	
1.751	$\begin{bmatrix}0.012 & 0.000 & 0.000\end{bmatrix}$
1.751	$\begin{bmatrix}0.000 & 0.012 & 0.000\end{bmatrix}$
1.751	$\begin{bmatrix}-0.012 & 0.000 & 0.000\end{bmatrix}$
1.751	$\begin{bmatrix}-0.000 & -0.012 & 0.000\end{bmatrix}$
0.516	$\begin{bmatrix}0.000 & 0.000 & 0.000\end{bmatrix}$
1.133	$\begin{bmatrix}0.010 & 0.010 & 0.000\end{bmatrix}$
1.133	$\begin{bmatrix}-0.010 & -0.010 & 0.000\end{bmatrix}$
1.133	$\begin{bmatrix}0.010 & -0.010 & 0.000\end{bmatrix}$
1.133	$\begin{bmatrix}-0.010 & 0.010 & 0.000\end{bmatrix}$

Table 2.2: Table of the vectors of $\mathcal{E}$, exclusing the mass-limited element.

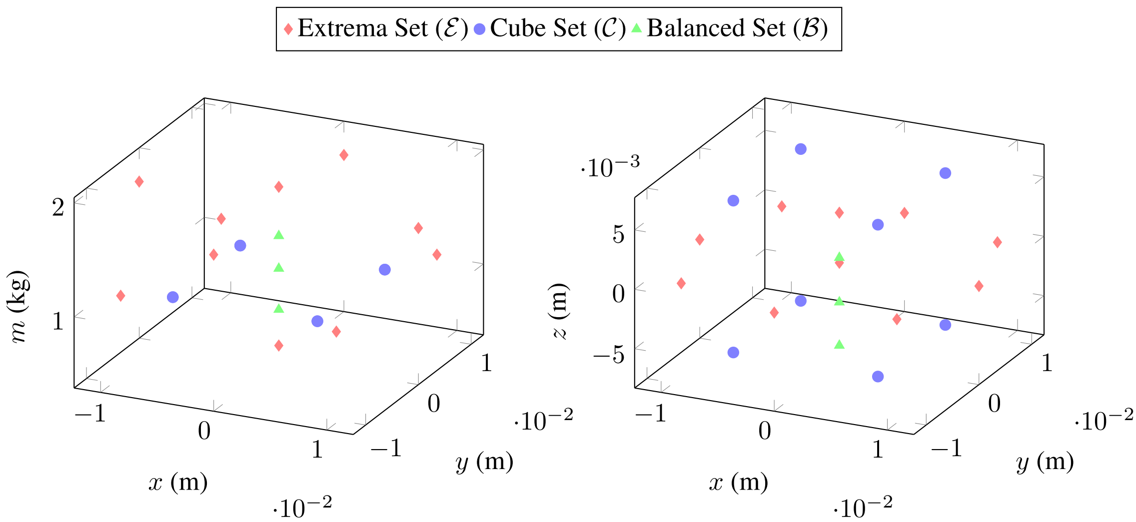

Figure 2.4: Mass and COM coordinates for each test point set.

Target		Nearest		L2 Norm Error
m	$\boldsymbol{r}$	m	$\boldsymbol{r}$	
Extrema Set ($\mathcal{E}$)				
2.000	$[0.000 \quad 0.000 \quad 0.000]$	1.909	$[0.000 \quad 0.000 \quad 0.004]$	9.154×10^{-2}
Cube Set ($\mathcal{C}$)				
$*$	$[-0.007 \quad -0.007 \quad -0.007]$	1.061	$[-0.006 \quad -0.006 \quad -0.006]$	1.055×10^{-3}
$*$	$[-0.007 \quad -0.007 \quad 0.007]$	1.061	$[-0.006 \quad 0.006 \quad -0.006]$	1.895×10^{-2}
$*$	$[-0.007 \quad 0.007 \quad -0.007]$	1.061	$[0.006 \quad -0.006 \quad -0.006]$	1.895×10^{-2}
$*$	$[-0.007 \quad 0.007 \quad 0.007]$	1.061	$[0.006 \quad 0.006 \quad -0.006]$	1.895×10^{-2}
$*$	$[0.007 \quad -0.007 \quad -0.007]$	1.061	$[-0.006 \quad -0.006 \quad 0.006]$	1.895×10^{-2}
$*$	$[0.007 \quad -0.007 \quad 0.007]$	1.061	$[-0.006 \quad 0.006 \quad 0.006]$	1.895×10^{-2}
$*$	$[0.007 \quad 0.007 \quad -0.007]$	1.061	$[0.006 \quad -0.006 \quad 0.006]$	1.895×10^{-2}
$*$	$[0.007 \quad 0.007 \quad 0.007]$	1.061	$[0.006 \quad 0.006 \quad 0.006]$	1.055×10^{-3}
Balanced Set ($\mathcal{B}$)				
0.516	$[0.000 \quad 0.000 \quad *]$	0.832	$[0.000 \quad 0.000 \quad -0.003]$	3.156×10^{-1}
1.258	$[0.000 \quad 0.000 \quad *]$	1.192	$[-0.000 \quad -0.000 \quad 0.000]$	6.630×10^{-2}
2.000	$[0.000 \quad 0.000 \quad *]$	1.478	$[-0.000 \quad -0.000 \quad -0.007]$	5.219×10^{-1}

Table 2.3: Table of the target and actual vectors for $\mathcal{C}$, $\mathcal{B}$ and the mass limited element of $\mathcal{E}$ with the L2 norm error. $*$ notation indicates "don't care" and is excluded from the search algorithm.

2.6 Conclusion and Discussion

References

[1] S. Kirkpatrick, C. D. Gelatt, and M. P. Vecchi, "Optimization by simulated annealing," *science*, vol. 220, no. 4598, pp. 671–680, 1983.

[2] P. Serafini, "Simulated annealing for multi objective optimization problems," in *Multiple criteria decision making*, Springer, 1994, pp. 283–292.

Chapter 3

Creating a Configurable Payload for Instability Experiments

3.1 Introduction

3.2 Control Experiments

3.2.1 Results

3.3 Conclusion and Discussion

No Tail $\begin{bmatrix}1.909 & 0.000 & 0.000 & 0.004\end{bmatrix}$

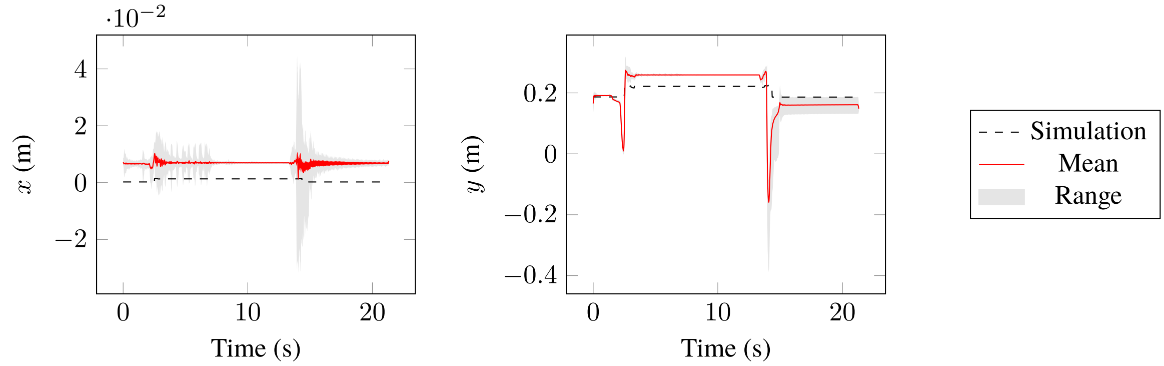

Figure 3.1: COM x and y position of the test rig along the test trajectory for the mass maximum element of the extrema set with no tail.

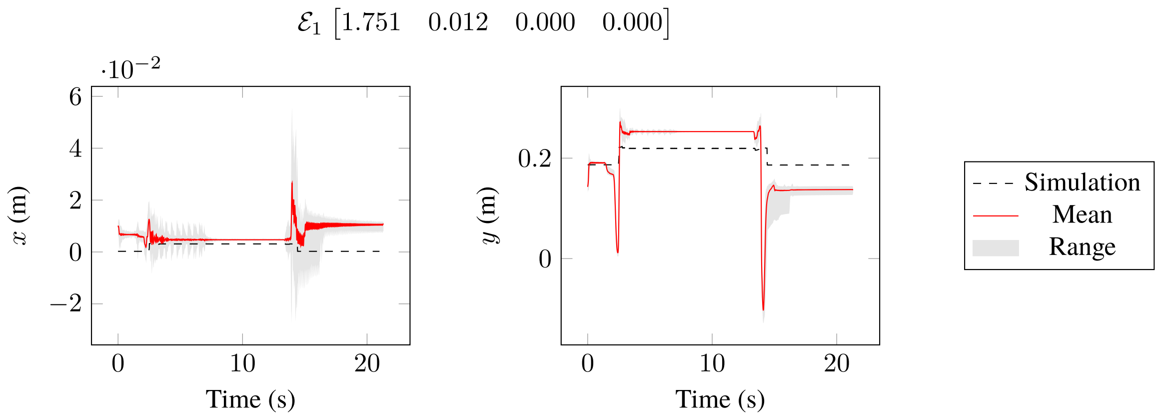

Figure 3.2: COM x and y position of the test rig along the test trajectory for the mass minimum element of the extrema set with no tail.

Chapter 4

Optimisation Study for Multi-Segment Tails for Centre of Mass Control

4.1 Introduction

One of the most noticeable differences between robotic and animal tails, as discovered in chapter **??**, is the far greater number of segments in most animal tails when compared to robot tails.

4.2 Model Definition

We can consider a tail with an arbitrary number of segments as a chain of bodies connected by revolute joints, where $\boldsymbol{l}$ are the lengths of the bodies, $\boldsymbol{m}$ are the masses of the bodies, $\boldsymbol{l_c}$ are the offsets of the COM from the origin of each body along the axis of the chain (assuming the COM remains on that axis for the sake of simplicity), and $\boldsymbol{\theta}$ are the angles of each revolute joint.

The transformation matrices for a given body's origin and COM can then be computed.

$$
\begin{aligned}
T_i &= \begin{bmatrix} \cos\theta_i & -\sin\theta_i & l_i \\ \sin\theta_i & \cos\theta_i & 0 \\ 0 & 0 & 1 \end{bmatrix} \\
T_{c_i} &= \begin{bmatrix} \cos\theta_i & -\sin\theta_i & l_{c_i} \\ \sin\theta_i & \cos\theta_i & 0 \\ 0 & 0 & 1 \end{bmatrix}
\end{aligned}
\tag{4.1}
$$

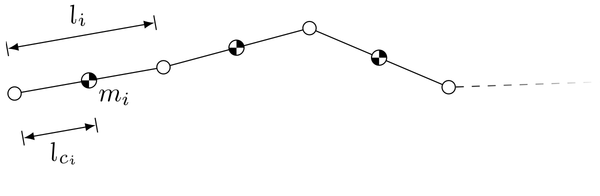

Figure 4.1: Diagram of a 2D tail, with all parameters annotated.

The forward kinematics for the tail is then computed. This will give us the position of the endpoint of the tail for a given set of joint angles $\boldsymbol{\theta}$.

$$T(\boldsymbol{\theta}) = \prod_{i=1}^{n} T_i \tag{4.2}$$

A similar equation can be used for the forward *kinetics*, with the addition of the body masses and COM offsets as parameters. This will give us the position of the COM for the entire tail.

$$R(\boldsymbol{\theta}) = \frac{\sum_{i=1}^{n} m_i \prod_{j=1}^{i-1} (T_j) T_{c_i}}{\sum_{i=1}^{n} m_i} \tag{4.3}$$

4.3 Inverse Kinetics

As we can compute the forward kinetics in a very similar fashion to the inverse kinematics, it follows that the inverse kinetics can be computed in a similar fashion. Firstly we define the Jacobian.

$$\boldsymbol{J}_R = \begin{bmatrix} \frac{\partial r_{13}}{\partial \theta_1} & \frac{\partial r_{13}}{\partial \theta_1} & \cdots & \frac{\partial r_{13}}{\partial \theta_n} \\ \frac{\partial r_{23}}{\partial \theta_1} & \frac{\partial r_{23}}{\partial \theta_1} & \cdots & \frac{\partial r_{23}}{\partial \theta_n} \end{bmatrix} \tag{4.4}$$

Then, assuming a COM position defined by $\begin{bmatrix} q_x & q_y \end{bmatrix}^\intercal$ the COM velocity can be calculated using the Jacobian.

$$\begin{bmatrix} \dot{q}_x \\ \dot{q}_y \end{bmatrix} = \boldsymbol{J}_R \cdot \dot{\theta} \tag{4.5}$$

To get the joint velocities instead for a given COM velocity, we can use a minimisation algorithm to calculate the optimal trajectory of $\boldsymbol{\theta}$ in order to minimise one or more undesirable aspects.

4.4 Minimisation Algorithms

4.4.1 Damped Least Squares

Damped Least Squares (DLS), also known as Levenberg-Marquardt [1], is perhaps one of the simplest algorithms to implement, giving

$$\dot{\boldsymbol{\theta}} = \boldsymbol{J}^\intercal \left(\boldsymbol{J}\boldsymbol{J}^\intercal \lambda^2 \boldsymbol{I} \right) \begin{bmatrix} \dot{q}_x \\ \dot{q}_y \end{bmatrix} \tag{4.6}$$

Where $\boldsymbol{I}$ is the identity matrix and λ is a suitable damping constant.

While it is easy to implement, DLS can only minimise the joint velocities, expressed as the euclidean norm $\|\dot{\boldsymbol{\theta}}\,(t)\,\|_2$.

4.4.2 Quadratic Programming

Quadratic programming

$$
\begin{aligned}
\boldsymbol{\tau} &= D\,(\boldsymbol{\theta})\,\ddot{\boldsymbol{\theta}} + C\left(\boldsymbol{\theta}, \dot{\boldsymbol{\theta}}\right) + G\,(\boldsymbol{\theta}) \\
\boldsymbol{Q} &= \alpha \boldsymbol{I} + (1-\alpha) D\,(\boldsymbol{\theta})^2 \\
\boldsymbol{p} &= \alpha \lambda \dot{\boldsymbol{\theta}} + (1-\alpha) D\,(\boldsymbol{\theta})^{\intercal} \left(C\left(\boldsymbol{\theta}, \dot{\boldsymbol{\theta}}\right) + G\,(\boldsymbol{\theta})\right) \\
\ddot{\boldsymbol{\theta}} &= \min_{\ddot{\boldsymbol{\theta}}} \frac{1}{2} \ddot{\boldsymbol{\theta}}^{\intercal} \boldsymbol{Q} \ddot{\boldsymbol{\theta}} + \boldsymbol{p}^{\intercal} \ddot{\boldsymbol{\theta}} \text{ s.t.} \left\{ \boldsymbol{J} \ddot{\boldsymbol{\theta}} = \ddot{x}_1 - \dot{\boldsymbol{J}} \dot{\boldsymbol{\theta}} \right.
\end{aligned}
\tag{4.7}
$$

4.5 Results

4.6 Conclusion and Discussion

References

[1] S. R. Buss, “Introduction to inverse kinematics with jacobian transpose, pseudoinverse and damped least squares methods,” *IEEE Journal of Robotics and Automation*, vol. 17, no. 1-19, p. 16, 2004.

Appendices